A Novel Closed-loop Architecture for Accurate Micromirror Trajectory Control in Linear Scanning MEMS-based Projectors

Paolo Frigerio[a], Riccardo Tarsi[a], Luca Molinari[b], Giuseppe Maiocchi[b], Andrea Barbieri[b], and Giacomo Langfelder[a]

[a]Politecnico di Milano, P.za Leonardo da Vinci, Milano, Italy
[b]STMicroelectronics, Via Tolomeo, Cornaredo (MI), Italy

ABSTRACT

In the field of raster scanning projectors, linear micromirrors used for image scan along the vertical axis are driven by a sawtooth waveform, whose frequency is related to image refresh rate (typically 60-120 Hz). Such driving profile with a fast retrace (10% of the period) excites the fundamental resonant mode, stimulating unwanted ringing of the tilt angle that worsens image quality, requiring a compensation. Open-loop solutions based on pre-distortion of the driving profile require accurate calibration of the device and do not offer enough versatility among different micromirrors. Embedded position sensors enable implementation of closed-loop techniques: this work presents an innovative linear control strategy for mirrors with piezoresistive position sensing, which allows to achieve accurate tracking of the control signal while suppressing resonance. The concept is based on a control approach: the goal is to damp the mirror quality factor, while achieving accurate tracking, within few tens of m°, and compensate for mechanical non-linearities by nulling the error between angle and control signal. An analog implementation is studied on a theoretical basis, to determine the fundamental limit in terms of tracking accuracy and noise. Then, a more versatile design is presented, where the controllers are implemented digitally to cover a wide range of mirror parameters. Analytical/behavioral simulations show the capability to achieve accuracy within 20 m°. Experimental testing on an analog implementation of the resonance damping loop proves the validity of the approach.

Keywords: MEMS, micromirror, projectors, linear, control, loop, PZT, piezoresistive

1. INTRODUCTION

Linear scanning micromirrors are employed in raster-scanning systems for projection along the vertical axis.[1] As such, these devices operate at typical working frequencies in the order of 60 Hz, equal to the image refresh rate. As the demand for increasing image resolution drives the need to increase the maximum field-of-view (FOV) and the mirror diameter, newer applications also demand to increase the working frequency. Given the required tight specifications, demanding a linearity of the projected trace and its reproducibility within 1% and 10 m°, respectively, and the increasing demand for higher refresh rates, accurate control of the mirror position becomes a challenge. Such a challenge is offered by the small resonance frequency of linear microscanners, justified by their typically large diameters in the order of a few mm, and their quality factor, in the order of 100, which generates undesired ringing of the mirror trajectory when the device is operated in open-loop conditions. To achieve the desired specifications it is thus mandatory to find solutions that eliminate ringing while also enabling accurate control and fast recovery from fast transients.

Different approaches have been shown in the literature, covering both open-loop and closed-loop control techniques. An interesting review of different control strategies, compared to experimental data, is provided by Milanović et al.[2] for the slow-axis of 2D gimbal-less electrostatically-actuated microscanners. Given the bandwidth of the devices, limited to a resonant frequency of about 800 Hz to 3 kHz, they showed the effectiveness

Further author information: (Send correspondence to P. Frigerio)
P. Frigerio: E-mail: paolo.frigerio@polimi.it
L. Molinari: E-mail: luca.molinari@st.com

of open-loop techniques, based on an inverse-system filter, and closed-loop techniques, enabled by an optical position sensor and based on a derivative controller, in damping the quality factor while retaining a system bandwidth in the order of the MEMS resonance frequency. Moreover, applying a simple PID controller they showed the possibility to extend the system bandwidth even beyond such value. Still concerning dual-axis mirrors, Juneau et al.[3] applied a non-linear controller, based on a PID (Proportional-Integral-Derivative) core, to overcome cross-axis limitations and compensate for intrinsic non-linearities when driving electrostatic mirrors with step signals, achieving settling times in the order of 10 ms. Janschek et al.[4] showed the effectiveness of open-loop adaptive techniques applied to comb-driven electrostatic microscanners to attain a reproducibility within 50 m°, which was further reduced to 3 m° by resorting to a more complex controller structure based on state observers. Tsai et al.[5] showed the implementation of a phase-lead controller to compensate the slow-axis of a 2D electromagnetic mirror, exploiting position sensing through a set of piezoresistive elements embedded on the mirror.

All these works are focused on electrostatic or electromagnetic scanners, adopting different types of position sensing, ranging from optical, to capacitive, to piezoresistive sensors. Electrostatic-driven devices need very large actuation voltages, often larger than 100 V, and show significant non-linearity in the actuation mechanism.[6–8] Electromagnetic devices, on the other hand, although showing improved linearity, require much larger area due to installation of permanent magnets in proximity of the device.[9,10] Significant improvements can be attained by switching to piezoelectric actuation, typically implemented by thin films of Lead-Zirconate-Titanate (PZT).[11,12] Piezoelectric actuation offers a significant reduction in actuation voltage, down to few tens of volts, and area occupation, while still retaining some non-linearity in the form of inherent hysteresis.[13]

In this work we present the design and implementation of an ASIC embedding a closed-loop control for quasi-static micromirrors based on piezoelectric actuation and piezoresistive position sensing. The target application is detailed in Section 2, along with the figures of merit used to evaluate the system performance. Section 3 describes modeling of the target mirrors and characterization of a sample device. Section 4 describes the digital-to-analog interfaces and the mirror drive and sense circuits. Section 5 describes the digital implementation of the proposed control strategy. Finally, section 6 shows results of system simulations performed using MATLAB/Simulink software.

2. TARGET APPLICATION AND PERFORMANCE METRICS

The ASIC is designed to cover a wide range of linear piezoelectric microscanners, with resonance frequencies ranging from 400 Hz to few kHz. The target operating frequencies are within 60 Hz and 120 Hz for triangular or sawtooth driving signals, with symmetric rise and fall times for the former, and a retrace smaller than and up to 20% of the signal period for the latter. Given the lower bound of the frequency range of interest, the controller is designed to achieve three results: first, it has to dampen the quality factor of the tilt mode in order to suppress position ringing; secondly, it has to increase the bandwidth of the closed-loop system in order to improve the linearity of the mirror response when the sawtooth frequency is increased to 120 Hz or larger and approaches the mechanical bandwidth; thirdly, it should guarantee good tracking of the reference signal, providing ideally a null error between controlled angle and reference. Implementation details concerning how these three goals are attained are given in the dedicated section. The controller is implemented as a digital processing unit, clocked at a rate in the order of hundreds of kHz, while the interfaces between analog and digital domains are clocked at a higher rate, in the order of MHz in order to exploit oversampling and thus reduce the in-band quantization noise.

Two metrics are used to assess the performance of the system: linearity and reproducibility of the trajectory. All these are evaluated considering the part of the trace used for projection, taken as 90% of the signal rising slope. Linearity is evaluated by taking the derivative of the trace $\theta(t)$ normalized to its average value:

$$L(t) = \frac{\dot{\theta}(t) - \underset{t}{\text{mean}}\left(\dot{\theta}(t)\right)}{\underset{t}{\text{mean}}\left(\dot{\theta}(t)\right)} \quad \text{for} \quad t \in (0.05 \cdot T_t, 0.95 \cdot T_t) \tag{1}$$

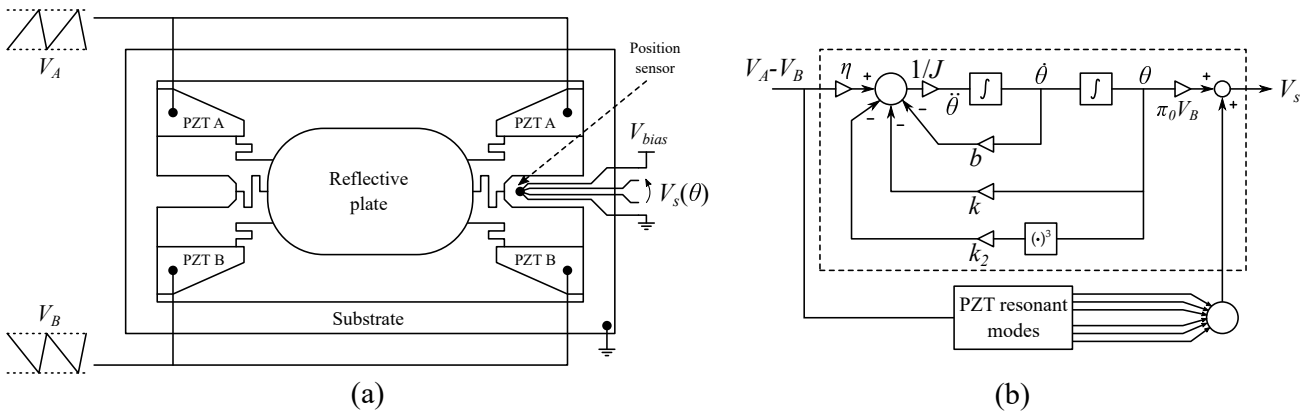

Figure 1. (a) Schematic top-view of a piezoelectric micro-mirror, showing the geometry of the PZT actuators, their electrical connection and the position of the piezoresistive sensor on the MEMS structure; (b) model of a generic piezoelectric micromirror.

where T_t is the trace time. Reproducibility is evaluated as the variation between the position at corresponding timestamps $t_j = t + jT$, where T is the signal period:

$$R(t_j) = \underset{t_j}{\text{std}} \left(\theta(t_j) - \underset{N}{\text{mean}} \left(\theta(t_j) \right) \right) \quad \text{for} \quad t_j \in (0.05 \cdot T_t, 0.95 \cdot T_t) \tag{2}$$

for a number N of subsequent traces.

3. MICROMIRROR MODEL AND CHARACTERIZATION

As schematically represented in Fig. 1(a), the body of a generic quasi-static piezoelectric mirror has a rectangular or ovoidal shape to accommodate the scan line generated by the associated resonant scanner, and is suspended by four piezoelectric actuators realized by deposition of a thin (2-µm) film of Lead-Zirconate-Titanate (PZT) on Silicon cantilevers, sandwiched between two biasing electrodes. The main mass with a reflective Aluminium coating is attached to the actuators via suitable folded springs.[14] The electrodes are connected in pairs, as indicated in the figure, to allow differential driving of the mirror. Each bottom electrode is tied to ground, while the top electrodes are biased with strictly positive voltages, phase shifted by 180°.

Additional torsional springs, along the longitudinal axis of the mirror, connect the main mass to large suspended Silicon beams that are anchored to the substrate. At the tip of one of the beams, close to the connection with the torsional spring, a set of four buried piezoresistors, realized by heavy n^+ doping, is diffused to allow sensing of the mirror position. These resistors, arranged in a Wheatstone bridge configuration, sense the stress generated by the mirror movement, providing an output voltage proportional to the instantaneous mirror tilt angle, when the bridge is properly biased by voltages in the order of 3 V.

Each mirror can thus be modeled according to Fig. 1(b), where the PZT actuators are modeled by a transformation coefficient η (units of Nm/V) that couples the electrical domain to the mechanical one. The latter is modeled by the well known spring-mass-damper model for torsional systems through the mechanical stiffness k (units N m), the damping coefficient b (units N m s), and the mass moment of inertia J (units kg m^2). The basic linear model is closed by the piezoresistive Wheatstone bridge, whose output voltage is proportional to the tilt angle θ by a piezoresistive coefficient π_0 (units rad^{-1}) linearly proportional to the stress, and the bias voltage V_B.

This model can be represented in the Laplace domain by a compact transfer function from the PZT drive voltage V_D to the piezoresistive sensor output voltage V_S, useful for the control system design:

$$H(s) = \frac{V_S}{V_D} = \frac{\eta \pi_0 V_B}{k + bs + Js^2} = \frac{H(0)}{1 + \dfrac{s}{\omega_n Q} + \dfrac{s^2}{\omega_n^2}} \tag{3}$$

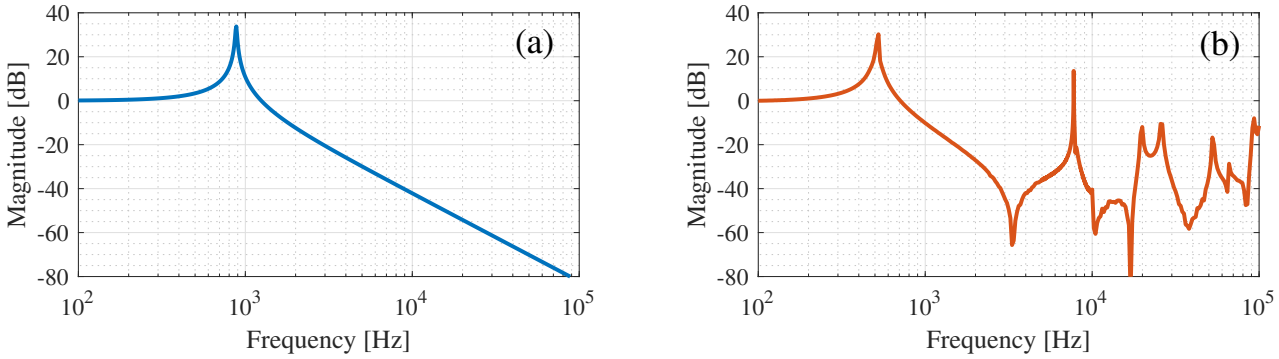

Figure 2. Magnitude of the transfer function from PZT drive voltage to piezoresistive sensor output voltage of an ideal micromirror (a) vs. a real micromirror (b) where significant coupling of high-frequency resonances can be observed. The effect of spurious resonances is modeled as complex-conjugate poles and zeros that can generate even within the control bandwidth.

where the gain $H(0)$, the natural frequency ω_n and the quality factor Q are defined as follows:

$$H(0) = \frac{\eta \pi_0 V_B}{k} \tag{4}$$

$$\omega_n = \sqrt{\frac{k}{J}} \tag{5}$$

$$Q = \frac{\omega_r J}{b}. \tag{6}$$

Moreover, as shown in Fig. 1(b), additional blocks are included to account for non-idealities that affect some mirror designs. First of all, due to the large opening angles, in the order of 7° and larger, the springs may show significant non-linearity, depending on the design. This is modeled by an additional contribution to the equation of motion, proportional to the cube of the tilt angle, or equivalently by a non-linear stiffness defined as:

$$k_{nl} = k + k_2 \theta^2 \tag{7}$$

where k is the linear stiffness and k_2 (units N m rad^{-3}) models the non-linear behavior.

Additionally, the effect of spurious high-frequency resonant modes is included as it is critical for a few particular designs. Regardless of the real shape of the resonant modes, be them out-of-plane translations or resonances of the actuator plates, their effect is modeled in terms of their coupling to the sensor output voltage. Such coupling may be stronger or weaker depending on key factors such as the sensor design and its final layout, as well as the type of motion. For example, in some designs a resonance of the actuators may be strongly coupled to the sensor output, due to residual stress exerted on the sensor. As it is easily understood, this problem adds an unwanted degree of complexity in the control strategy, as the information provided by the sensor output is corrupted by resonance-induced disturbances which have to be filtered out to properly control the mirror rotation. The spurious mode coupling is modeled by altering the transfer function in equation (3) and modeling the output of the piezoresistive sensor as a sum of second-order transfer functions:

$$H_M(s) = \sum_{j=1}^{M} \frac{\eta_j}{k_j} \cdot \frac{\pi_{0j} V_B}{1 + \dfrac{s}{\omega_{nj} Q_k} + \dfrac{s^2}{\omega_{nj}^2}} \tag{8}$$

where M is the number of mechanical resonances coupled to the output (including the roll mode), and the subscript j indicates the parameters of the j-th eigenfrequency.

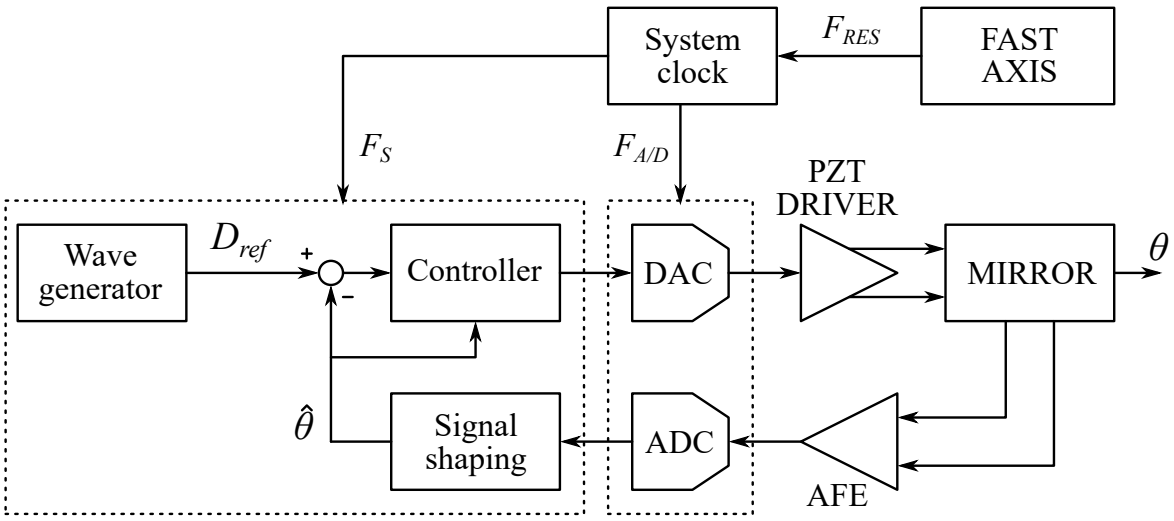

Figure 3. Block diagram of the ASIC.

Finally, since the spurious high-frequency modes do not correspond to a real rotation of the mirror, the transfer function from actuation voltage to tilt angle is defined as:

$$H_\theta(s) = \frac{\eta_1}{k_1} \cdot \frac{1}{1 + \dfrac{s}{\omega_{n1} Q_1} + \dfrac{s^2}{\omega_{n1}^2}} \tag{9}$$

where the electro-mechanical parameters denoted with subscript 1 are characteristic of the roll mode. Fig. 2 shows the expected transfer function for a mirror design where spurious modes have a negligible effect, derived by FEM simulations, compared to the measured transfer function (acquired via network analyzer) of a mirror with non-negligible spurious modes.

4. ASIC DESCRIPTION: DIGITAL-TO-ANALOG INTERFACES AND DRIVER

The block scheme of the ASIC designed to control the slow axis is represented in Fig. 3. Aside from the controller and the wave generator, described in the following section, the chip contains a DAC for converting the controller output into the analog domain, a power amplifier to drive the PZT actuators, an analog front-end (AFE) for the readout of the Wheatstone bridge output and an ADC to convert the AFE output into a digital number that can be processed by the controller.

The digital-to-analog converter is based on a third-order $\Delta\Sigma$ modulator (referred to as DSM in the following), followed by a current-steering DAC and two first-order analog low-pass filters (LPF). The controller output signal, clocked at a few hundreds kHz (dependent on the resonant mirror frequency, as explained in the following), is up-sampled to a few MHz to exploit oversampling. This signal is processed by the modulator, whose output bitstream (1-bit) is filtered by a FIR filter implementing a moving average. Its 32 unit-gain taps are used to steer an equal number of current generators between the two input terminals of a fully-differential trans-impedance amplifier (TIA), implementing the first LPF, whose output is then filtered by a second LPF to further attenuate high-frequency noise. The bandwidth of the entire converter is about 50 kHz.

The piezoelectric driver is a power amplifier that generates anti-phase signals to control the two sets of PZT actuators, amplifying the low-voltage DAC output up to the 40 V required to achieve the desired mirror tilt angles. The amplifier needs to drive actuators with capacitances up to 50 nF for the most demanding mirror designs, and thus, in order to maintain stability, its bandwidth is limited to about 10 kHz in such worst-case conditions.

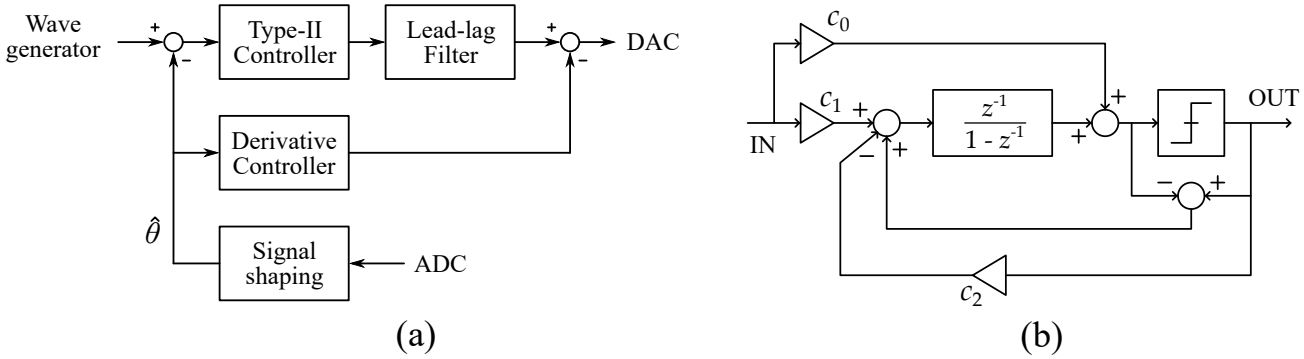

Figure 4. (a) Block diagram of the digital controller, showing the signal shaping block processing the output of the ADC, the "inner" derivative loop, and the position controller constituted by the integrator and lead-lag filter; (b) filter topology used to implement all the controller filters.

The analog front-end is made by a cascade of two programmable gain stages, to allow management of different opening angles and piezoresistive sensor sensitivities. The bandwidth of this stage is large enough (about 2.5 MHz) to be negligible when designing the control loop.

The analog-to-digital converter is based on a second-order $\Delta\Sigma$ topology for linearity. The sampling frequency is the same as for the DAC, and following the converter is a third order decimation filter with programmable bandwidth to attenuate quantization noise. The frequency is thus downscaled to the clock rate used to update the control law.

At the end of the sense path is a cascade of four programmable biquadratic filters, whose purpose is explained in the next section. This is of particular importance for the management of spurious resonance modes.

5. CONTROL LAW AND DIGITAL IMPLEMENTATION

Damping of the quality factor is achieved by implementing a differentiator loop, as shown in Fig. 4(a), that essentially controls the velocity of the mirror. By properly setting the derivative block and the gain it is possible to move the complex-conjugate poles of the mechanical response close to the real axis, effectively obtaining a quality factor smaller than $\sqrt{2}/2$. The bandwidth of the compensated plant remains the same as the mechanical bandwidth, if the controller is properly sized.

Extension of the bandwidth is achieved implementing a lead-lag controller that manages the compensated plant. The coefficients of the lead-lag filter can be tuned in order to ideally achieve an arbitrary extension of the system bandwidth. It should be noted, however, that the bandwidth can not be extended indefinitely, as larger bandwidth means larger noise. As a rule of thumb, in order to achieve good accuracy the closed-loop bandwidth should be extended beyond at least 3 kHz, with low-frequency mirrors being the most demanding in reaching this goal. With such a sizing, roughly 25 harmonics of a 120-Hz sawtooth signal fall within the closed-loop bandwidth.

Minimization of the tracking error is also achieved by including two integrators in the controller of the compensated plant. Since the reference signal is a ramp (within one period), two integrators are required by control theory to render the steady state loop error ideally null. The controller has to be designed in order to guarantee the fastest possible transient recovery time at the beginning of the trace, in order to be compliant with the linearity spec. As an additional beneficial effect, if the effect of spurious modes is negligible the integrators effectively reject the geometric non-linearity of the mirror, given the linearity of the piezoresistive sensor and the nulling of the loop error.

Every filter is implemented as a fully programmable first order digital filter, adopting the structure represented in Fig. 4(b). This structure includes an anti-windup scheme to prevent prolonged saturations due to the presence of two integrators in the control loop. An additional lead-lag filter is placed at the end of the signal path, before

the DAC, in order to boost the phase margin in scenarios where the bandwidth of the high-voltage driver is limited to 10 kHz.

In cases where the effect of high-frequency modes is not negligible, as the one presented in Fig. 2, additional care has to be taken in order to avoid instability of the system. To this purpose, the set of four biquadratic filters described in the previous section can be used to pre-condition the feedback signal before using it to calculate the controller output. Given the requirement to extend the system bandwidth, the effect of modes visible up to frequencies of 8 kHz is detrimental as they pose a serious limitation to the achievable closed-loop bandwidth, particularly for low-frequency mirrors. Additionally, the combined effect of the spurious poles with the tilt mode may generate additional zeros that may even prohibit any significant bandwidth extension, thus invalidating many mirror design choices just because they lead to a relatively small mechanical bandwidth.

The proposed solution does not simply notch the resonance poles, but also aims at compensating the zeros with a sufficient degree of accuracy to maintain system stability even in such harsh conditions, effectively implementing a shaping of the mirror transfer function. The overall shaping filter $H_F(s)$ of Fig. 4 is thus realized by setting:

$$H_F(s) \cdot H_M(s) = H_1(s) \tag{10}$$

where $H_1(s)$ is the transfer function of equation (3). With such definition the filter is always proper, and the number of both poles and zeros to implement is equal to the number of spurious resonances. Clearly it is not required to apply a shaping to every resonant mode, but only to the ones that may be harmful for the stability of the system and the requirement of bandwidth extension. Thus, only four filters have been allocated to save area, but also to enable control of different mirror families.

The signal generator samples the reference waveform from a table of 32 samples, that are up-sampled to the controller clock frequency by a third order interpolator. When the controlled plant yields a closed-loop bandwidth unable to attain the desired linearity performance, the samples can be defined to compensate for any over/undershoot in the mirror response by artificially increasing the bandwidth providing a pre-shaping of the waveform. This shaping is obtained by applying an inverse-system filter, tailored to the closed-loop transfer function. Differently from Ref. 2, implementation of such filter is eased by the controller, requiring a less accurate model of the mirror resonance frequency and of the quality factor. The reference waveform is thus generated by applying the following filter to the ideal reference waveform, before storing its samples in the table:

$$F(s) = \frac{H_{cl}^{-1}(s) \cdot \widehat{H}(s)}{P(s)} \tag{11}$$

where $H_{cl}(s)$ is the closed-loop transfer function after application of the controllers, $\widehat{H}(s)$ is the desired closed-loop transfer function (i.e. two real coincident poles), and $P(s)$ introduces additional high-frequency poles to make the filter proper, if needed.

6. SIMULATION RESULTS

Simulation results are shown for two designs of a mirror with a nominal resonance frequency of 880 Hz. The two samples differ for the different transfer function. Both mirrors are driven by a sawtooth signal having 120-Hz frequency and retrace equal to 20% of the period. Their transfer functions are reported in Fig. 5.

Fig. 6(a) shows a comparison between the obtainable linearity, extracted from the simulated trace as described in Section 2. If the mirror has no significant spurious modes within the control bandwidth, the expected linearity attained by the proposed system can be smaller than 1%. However, if the high-frequency modes are coupled to the sensor output, the proposed strategy leads to a worsening of the linearity.

Fig. 6(b) shows comparison between the trace reproducibility in the two cases. The expected position error attained by the system with no significant spurious modes is aligned with theoretical predictions of the angle RMS noise, designed to be smaller than 10 m° RMS. However the presence of spurious modes, and thus their compensation, increases the total noise up to 12 m° RMS.

These results, although requiring an experimental validation, show a theoretically achievable linearity and noise within 1% RMS and 5 m° RMS, respectively, and the limitations of the proposed control approach when limited by high-frequency spurious resonances, that lead to a worsening of both linearity and noise.

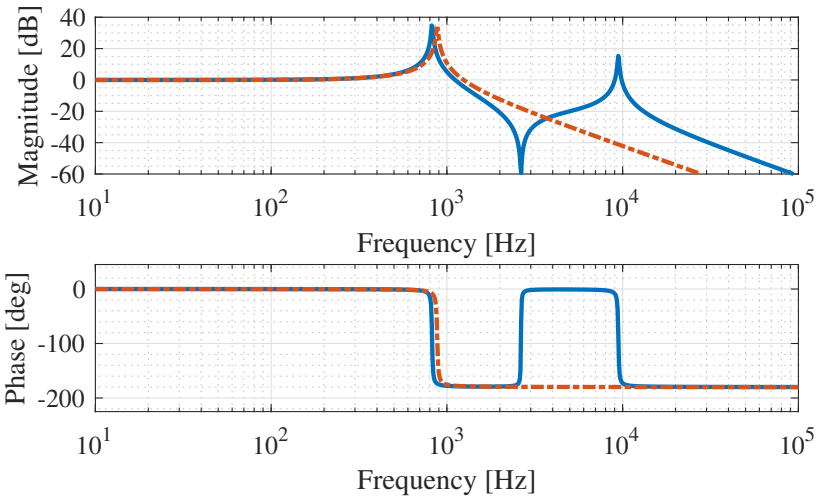

Figure 5. Transfer function of a mirror with no significant spurious modes (dashed orange line), compared to the transfer function of a mirror with a significant mode at about 10 kHz (solid blue line) coupled to the piezoresistive sensor output.

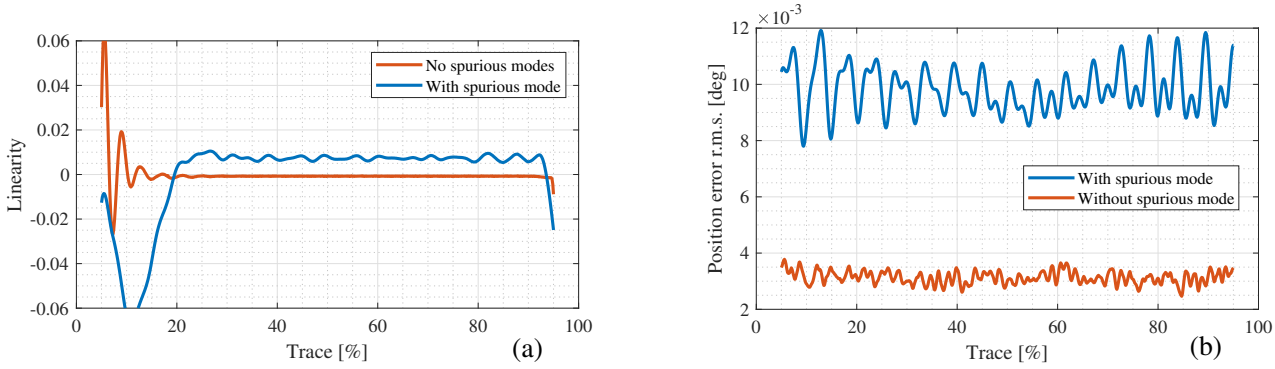

Figure 6. (a) Comparison between the linearity attained with the two simulated mirrors. The RMS of this trace rises from 0.7% when no significant spurious resonance is present, up to 1.82% for the case with a significant mode at 10 kHz; (b) comparison between the reproducibility attained with the two simulated mirrors. The point-to-point RMS position error increases from about 3 m° to about 12 m° when introducing spurious modes.

7. PRELIMINARY EXPERIMENTAL VALIDATION

A preliminary validation of the approach was carried out implementing the system on a printed board, using commercially available discrete components and the controller implemented with analog circuitry. With such setup, a preliminary validation of the derivative control was carried out. The transfer function of the tested mirror is the one shown in Fig. 2(b). The device was actuated with a 60-Hz triangle signal with 90%-trace/10%-retrace provided by an arbitrary waveform generator.

Fig. 7 shows a comparison between the open-loop and closed-loop transfer function from the reference signal to the output of the analog front-end (implemented by a low-noise Instrumentation Amplifier), acquired via a Network Analyzer. The plot shows the damping of the quality factor. The corresponding time-domain responses are also shown in Fig. 8(a).

Fig. 8(b) shows the linearity extracted from the closed-loop response shown in Fig. 8(a), showing that a simple derivative control is unable to provide the required linearity when driving mirrors with a 500 Hz resonance frequency, which was expected from theoretical and simulation results.

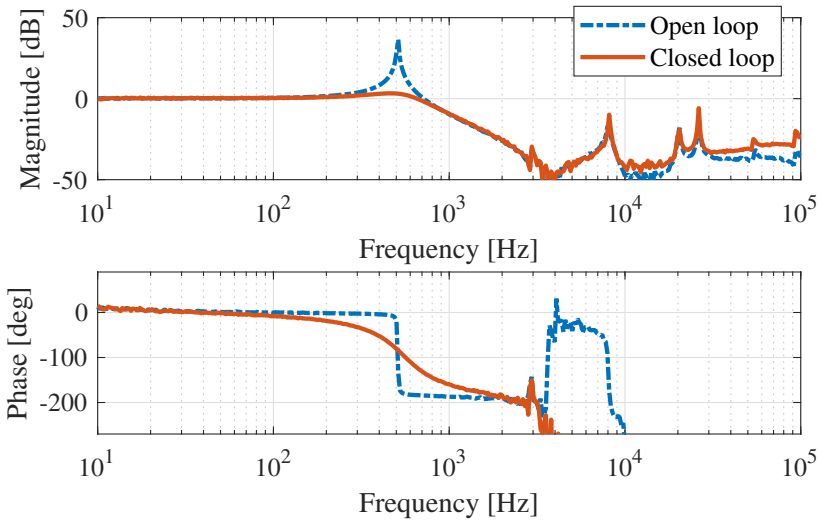

Figure 7. Normalized experimental transfer function (from reference signal to front-end output) in open-loop and closed-loop conditions with an applied derivative controller.

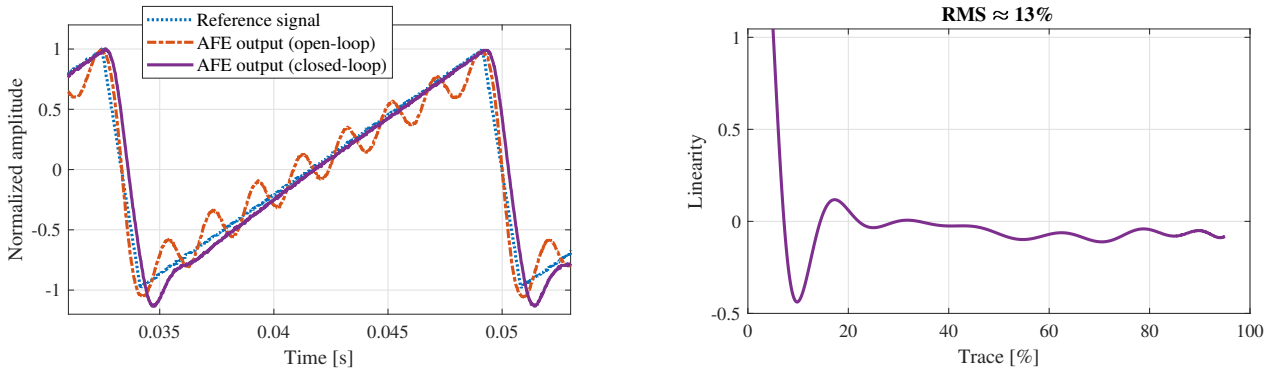

Figure 8. (a) Time-domain normalized response of the analog system. The open-loop and closed-loop waveforms are acquired at the output of the sensor front-end, acquired via oscilloscope; (b) trace linearity extracted from measured data (closed-loop), filtered to remove oscilloscope quantization. Regardless of such quantization, the measured linearity is still quite large, with an RMS in the order of 13%.

8. CONCLUSION AND FUTURE WORK

This work has detailed the design and implementation of an ASIC for position control of linear micromirrors with piezoelectric actuation and an embedded piezoresistive position sensor. The chip was designed to allow control of a wide range of mirrors. The control law was designed in order to suppress the ringing due to the large quality factor of the roll mode, while extending the closed-loop bandwidth in order to properly control mirrors with resonance frequencies down to 500 Hz with sawtooth signals having 120 Hz or higher frequency. The chip was also designed to manage mirrors with non-negligible spurious resonance modes that are coupled to the output of the position sensor. Simulation results prove the validity of the proposed approach, although showing a worsening of the performance due to high-frequency modes. Future work will focus on the experimental validation of the design, aimed at investigating the intrinsic limitations of the proposed approach. Furthermore alternative solutions will be studied to bypass these limitations, and thus improving the system robustness to spurious resonances.

REFERENCES

[1] Holmström, S. T., Baran, U., and Urey, H., "Mems laser scanners: a review," *Journal of Microelectromechanical Systems* **23**(2), 259–275 (2014).

[2] Milanović, V., Kasturi, A., Yang, J., and Hu, F., "Closed-loop control of gimbal-less MEMS mirrors for increased bandwidth in LiDAR applications," in [*Laser Radar Technology and Applications XXII*], **10191**, 101910N, International Society for Optics and Photonics (2017).

[3] Juneau, T., Unterkofler, K., Seliverstov, T., Zhang, S., and Judy, M., "Dual-axis optical mirror positioning using a nonlinear closed-loop controller," in [*TRANSDUCERS'03. 12th International Conference on Solid-State Sensors, Actuators and Microsystems. Digest of Technical Papers (Cat. No. 03TH8664)*], **1**, 560–563, IEEE (2003).

[4] Janschek, K., Sandner, T., Schroedter, R., and Roth, M., "Adaptive prefilter design for control of quasistatic microscanners," *IFAC Proceedings Volumes* **46**(5), 197–206 (2013).

[5] Tsai, C.-C., Li, Z.-H., Lin, Y.-T., and Lu, M. S.-C., "A Closed-Loop Controlled CMOS MEMS Biaxial Scanning Mirror for Projection Displays," *IEEE Sensors Journal* **20**(1), 242–249 (2019).

[6] Silva, G., Carpignano, F., Guerinoni, F., Costantini, S., De Fazio, M., and Merlo, S., "Optical detection of the electromechanical response of mems micromirrors designed for scanning picoprojectors," *IEEE Journal of Selected Topics in Quantum Electronics* **21**, 147–156 (July 2015).

[7] Jung, D., Sandner, T., Kallweit, D., and Schenk, H., "Vertical comb drive microscanners for beam steering, linear scanning, and laser projection applications," in [*MOEMS and Miniaturized Systems XI*], Schenk, H., Piyawattanametha, W., and Noell, W., eds., **8252**, 232 – 241, International Society for Optics and Photonics, SPIE (2012).

[8] J.-W. Cho et al., "Electrostatic 1D microscanner with vertical combs for HD resolution display," in [*MOEMS and Miniaturized Systems VI*], **6466**, 106 – 117, International Society for Optics and Photonics, SPIE (2007).

[9] Yalcinkaya, A. D., Urey, H., Brown, D., Montague, T., and Sprague, R., "Two-axis electromagnetic microscanner for high resolution displays," *Journal of Microelectromechanical Systems* **15**, 786–794 (Aug 2006).

[10] Muyu Chen, Huijun Yu, Shuai Guo, Run Xu, and Wenjiang Shen, "An electromagnetically-driven mems micromirror for laser projection," in [*10th IEEE International Conference on Nano/Micro Engineered and Molecular Systems*], 605–607 (April 2015).

[11] Masanao Tani, Masahiro Akamatsu, Yoshiaki Yasuda, and Hiroshi Toshiyoshi, "A two-axis piezoelectric tilting micromirror with a newly developed pzt-meandering actuator," in [*2007 IEEE 20th International Conference on Micro Electro Mechanical Systems (MEMS)*], 699–702 (Jan 2007).

[12] Dahl-Hansen, R. P., Tybell, T., and Tyholdt, F., "Performance and reliability of pzt-based piezoelectric micromirrors operated in realistic environments," in [*2018 IEEE ISAF-FMA-AMF-AMEC-PFM Joint Conference (IFAAP)*], 1–4 (2018).

[13] Vautier, B. J. G. and Moheimani, S., "Charge driven piezoelectric actuators for structural vibration control: issues and implementation," *Smart materials and structures* **14**(4), 575 (2005).

[14] Frigerio, P., Di Diodoro, B., , Rho, V., Carminati, R., Boni, N., and Langfelder, G., "New wide-angle micromirror with PZT actuation and PZR sensing," *Journal of Microelectromechanical Systems* (2021).